Research Article Vol. 8, No. 6 / June 2021 / Optica 861

optica

Chirped dissipative solitons in driven optical resonators

CHRISTOPHER SPIESS, QIAN YANG, XUE DONG, VICTOR G. BUCKLEW, AND WILLIAM H. RENNINGER*

Institute of Optics, University of Rochester, Rochester, New York 14627, USA
**Corresponding author: william.renninger@rochester.edu*

Received 13 January 2021; revised 20 April 2021; accepted 29 April 2021 (Doc. ID 419771); published 10 June 2021

Solitons are self-sustaining particle-like wave packets found throughout nature. Optical systems such as optical fibers and mode-locked lasers are relatively simple, are technologically important, and continue to play a major role in our understanding of the rich nonlinear dynamics of solitons. Here we present theoretical and experimental observations of a new class of optical soliton characterized by pulses with large and positive chirp in normal dispersion resonators with strong spectral filtering. Numerical simulations reveal several stable waveforms including dissipative solitons characterized by large frequency chirp. In experiments with fiber cavities driven with nanosecond pulses, chirped dissipative solitons matching predictions are observed. Remarkably, chirped pulses remain stable in low quality-factor resonators despite large dissipation, which enables new opportunities for nonlinear pattern formation. By extending pulse generation to normal dispersion systems and supporting higher pulse energies, chirped dissipative solitons will enable ultrashort pulse and frequency comb sources that are simpler and more effective for spectroscopy, communications, and metrology. Scaling laws are derived to provide simple design guidelines for generating chirped dissipative solitons in microresonator, fiber resonator, and bulk enhancement cavity platforms.

https://doi.org/10.1364/OPTICA.419771

1. INTRODUCTION

Self-organizing structures are found in many natural nonlinear systems including the ocean, the atmosphere, solid-state matter, and animals [1]. Optical systems have played a major role in the study of self-organization, including with the development of solitons, which are self-sustaining pulses with fascinating particle-like properties and technological importance including for lasers and telecommunications. Early studies of solitons, such as in optical fibers, assumed a lossless medium and a conservative balance between dispersive (or diffractive) effects and nonlinearity. However, it was later discovered that solitons can also form in the presence of dissipation if an external energy source is continuously supplied to the system. These dissipative solitons are found in electrical transport systems, chemical solutions, nerve pulses, and optical systems [2]. Dissipative solitons in driven optical cavities in particular have attracted considerable interest because they enable stable optical frequency combs with large frequency spacings spanning more than an octave [3–5] for applications in waveform synthesis, high-capacity telecommunications, astrophysical spectrometer calibration, atomic clocks, and dual-comb spectroscopy [6,7]. Dissipative cavity solitons were studied in fiber cavities [8–16] before development in micron-scale resonators [17–21] and most recently in bulk enhancement cavities [22,23].

Solitons in optical resonators are closely related to the solitons in optical fibers and in mode-locked lasers [24] where the Kerr optical nonlinearity balances with anomalous group-delay dispersion (GDD) to enable invariant propagation of the wave packet. The dissipation, which is typically designed to be small (~1% in microresonators), plays a relatively minor role in pulse formation and key pulse parameters can be predicted by neglecting dissipation [21,25,26]. However, in mode-locked laser cavities with normal dispersion and a spectral filter, a distinct class of frequency-chirped soliton can be generated where dissipation is essential for pulse formation [16,27–30]. In addition to inspiring studies of pulse formation with strong internal energy flows, chirped-pulse solitons in lasers have benefited applications by extending pulse generation to normal dispersion systems, enabling orders of magnitude larger pulse energies [31] and simplifying amplifier designs [32]. If chirped dissipative solitons can be generated by driven-resonator systems, opportunities for nonlinear pattern formation and improvements to performance comparable to those in chirped-pulse lasers are expected. However, translating solutions from mode-locked lasers to Kerr resonators is highly nontrivial; it took three decades to observe an analogy to the traditional soliton from mode-locked lasers in Kerr resonators. Kerr resonators are governed by distinct nonlinear differential equations that support solitons with very different internal energy flows. Moreover, little is known about the relevant governing nonlinear equation modeling filtered normal dispersion Kerr resonators. To date, despite several studies exploring anomalous [33,34] and

normal [35–45] dispersion cavities, chirped dissipative solitons have not yet been observed in Kerr resonators. In one notable study, normal dispersion microresonators were examined with a weak frequency dependent loss [45]. While the observed temporal signature is slightly longer (34%) than the transform-limited pulse, the measurements are consistent with noisy states in Kerr resonators [46,47], and the drive power is several orders of magnitude lower than the threshold power for stable chirped dissipative solitons established in this study.

Here we experimentally and numerically observe chirped dissipative solitons in driven normal dispersion fiber cavities with specifically designed spectral filtering. In stark contrast to traditional resonator solitons, chirped solitons are unstable without loss and are stabilized in resonators with >50% dissipation per round trip. Numerical simulations reveal stable bright optical pulses with chirp corresponding to more than twice the linear dispersion of the cavity and the potential for more than an order of magnitude higher energies than can be supported by traditional solitons. Chirped solitons, in agreement with predictions, are observed in experiments with long normal dispersion fiber cavities driven with nanosecond pulses. Stable chirped pulse formation in the presence of such strong dissipation paves the way for realizing high energy dissipative soliton resonances [48] and exotic nonlinear behavior such as dissipative soliton explosions [49,50] in passive resonators. The higher pulse energies enabled by chirped dissipative solitons can lead to improved resolution, signal-to-noise, and power for microcomb applications. In fiber resonators, chirped dissipative solitons offer the potential for generating ultrafast pulses at wavelengths where traditional sources cannot, complementing them for applications including biomedical imaging and spectroscopy. Finally, bulk normal dispersion cavities with a filter complement traditional enhancement cavities [22,23] by enabling chirped dissipative solitons relying on highly dissipative pulse shaping for improved high harmonic generation, temporal and spectral coherence enhancement, and pulse compression at the highest energy scales. Scaling laws are developed for designing chirped dissipative solitons for each of these platforms to enable a broad new range of system and performance parameters for ultrashort pulse and frequency comb generation.

2. RESULTS

A. Theory

A passive fiber resonator with normal dispersion and spectral filtering is analyzed numerically to determine whether chirped dissipative solitons can be stabilized (see Supplement 1, Section 1). The cavity consists of normal dispersion fiber, losses, a drive source, and a spectral filter [Fig. 1(a)]. After the fiber section, modeled by a detuned nonlinear Schrödinger equation, the loss, drive, and spectral filter are added as lumped elements (more details in Supplement 1, Section 1). The spectral filter (a Gaussian profile with 4 nm bandwidth) is chosen based on the requirements for a mode-locked fiber laser with the same cavity length (52.5 m in this case) [29,51]. After fixing the filter, cavity length, and losses, the simulations are examined as a function of the remaining variables: the intra-cavity drive peak power and frequency (cavity detuning). First, the trivial continuous-wave solutions and solutions that do not converge are indicated by white regions in Fig. 1(b) (see Supplement 1, Sections 3 and 4). To identify nontrivial solutions, multiple characteristics are examined, including the spectral bandwidth, peak power, chirp, and number of prominent intensity peaks (see Supplement 1, Section 5). The number of peaks in the converged waveform provides particularly good contrast between different solution types [Fig. 1(b)]. A variety of stable nontrivial solutions are observed, including chirped pulses, dark pulses, switching-waves, and Turing patterns. In Fig. 1(b), the Turing patterns, with more than eight intensity peaks, are indicated with red points, and the dark pulses, switching waves, and chirped pulses, which can occur with a single peak, are indicated with blue points. The different nonlinear solutions can also coexist (see Supplement 1, Section 6). The chirped dissipative solitons of interest exist over a broad range of detuning and drive power values, including both signs of detuning. Note that because the detuning is 2π periodic in this model, 0 detuning can also be interpreted as -2π detuning from the neighboring resonance. The minimum (threshold) intra-cavity peak drive power for which chirped pulses are observed is 5 W, defined as the power that is coupled into the cavity after a 5% coupler. The dynamics and stability regions of all of the solutions change significantly when the spectral filter bandwidth changes. For example, for chirped pulses, the threshold drive power decreases with narrower filter bandwidths. Moreover, the chirped pulses are not observed at all with broadband or without spectral filtering (see Supplement 1, Section 7).

The chirped-pulse solitons rapidly converge to a steady state in the cavity [Fig. 2(a) and Supplement 1, Section 3]. In the example illustrated in Fig. 2, the picosecond pulses exhibit a positive chirp corresponding to 1 ps^2 of GDD [Fig. 2(b) and Supplement 1, Section 1]. This corresponds to more than double the GDD of the normal dispersion fiber in the cavity, which indicates that the chirp is the result of nonlinear pulse formation. The dechirped pulse peak power is enhanced by a factor of ~4 from its value directly out of the cavity [Fig. 2(c)]. The pulses can be compressed to 0.9 ps, which is close to the transform-limited pulse duration of 0.82 ps and indicates that the chirp is nearly linear. The duration and chirp of chirped dissipative solitons vary depending on the bandwidth of the spectral filter (see Supplement 1, Section 8).

The spectral bandwidth, temporal duration, and chirp magnitude evolve nonlinearly in the cavity [Fig. 2(d)]. In the normal dispersion waveguide, the spectrum experiences a net broadening due to Kerr self-phase modulation. The temporal width increases primarily owing to dispersive propagation in the normal dispersion waveguide. The spectral filter reduces the spectral bandwidth, and the pulse duration is also reduced when the high and low frequencies in the leading and trailing edges of the pulse are attenuated. The pulse is highly chirped at every point in the cavity. This can also be seen from the positive slope of the instantaneous frequency on the right of Fig. 2. The dissipative drive and losses have a negligible effect on the pulse, spectrum, and chirp. Overall, the qualitative balance of physical effects is similar to that in chirped-pulse mode-locked lasers, in which pulse and spectral broadening are also counteracted by spectral filtering [29,51] (see Supplement 1, Section 9). However, we note that the continuous-wave background (absent in mode-locked lasers) has a time-dependent phase relationship with the chirped pulse, which results in an oscillatory structure in the time domain that can complicate the interpretation of the evolution. In this case, the chirped dissipative solitons are stable despite a total of 69.5% loss in one round trip, which is in large part due to the spectral filter (the typical loss at the center frequency is 21.5%, corresponding to a Q of 1.3 billion and a finesse

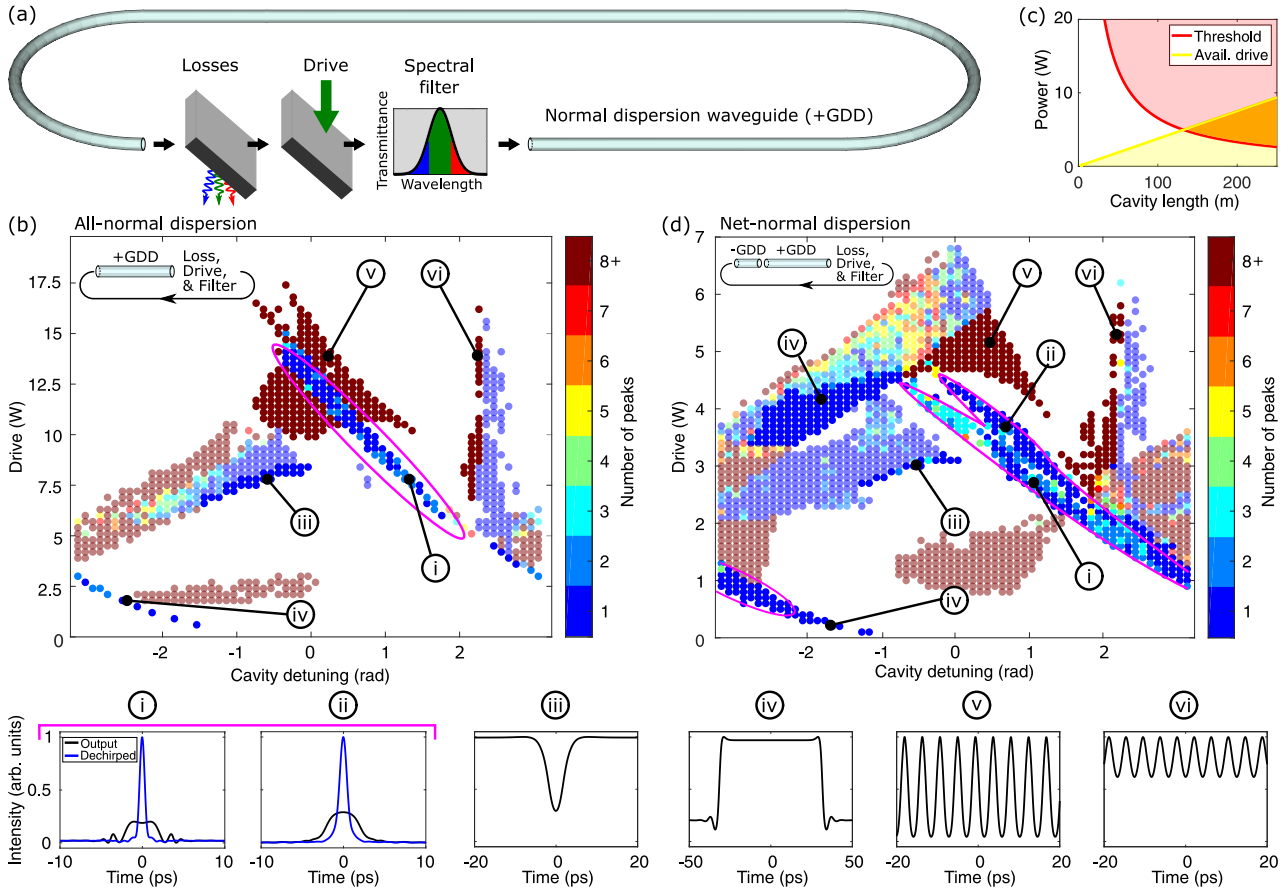

Fig. 1. Cavity design for chirped dissipative soliton generation and numerical results. (a) Illustration of the key components for observing chirped pulses in driven resonators, including a normal dispersion waveguide, losses, a drive, and a spectral filter. (b) Converged solutions as a function of intra-cavity drive power and detuning for an all-normal dispersion cavity. The color map represents the number of prominent peaks on the stable waveform. Specific solutions are indicated with Roman numerals. (i), (ii) Chirped pulses are observed in a well-defined region of parameter space (pink outline), and (iii) dark pulses, (iv) switching waves, and (v), (vi) Turing waves are observed elsewhere. (c) The minimum cavity length required for observing chirped solitons (orange) is determined by the decreasing threshold power (red) and the increasing available peak drive power (yellow) as a function of length. (d) Converged solutions as a function of intra-cavity drive power and detuning comparable to (b) for the cavity with large net-normal dispersion developed experimentally. See Supplement 1, Section 2 for cavity parameters.

of 26). Depending on the specific cavity arrangement, including the specific coupling losses and filter bandwidth, chirped dissipative solitons are observed with at least 92% round trip intra-cavity losses (see Supplement 1, Section 10).

Simple scaling laws can be developed to identify the cavity parameters necessary to obtain chirped-pulse solutions in driven-cavity systems. This is achieved by approximating the non-distributed cavity using a modified form of the well-established mean-field model for the driven-cavity system, the Lugiato–Lefever equation (LLE). To account for additional spectral filtering a term that represents a distributed Gaussian spectral filter is added (see Supplement 1, Section 11). The normalized equation can be defined by the following three unitless coefficients related to the intra-cavity peak drive power, spectral filter bandwidth, and drive detuning:

$$D_{n0} = D\frac{\gamma L}{\alpha^3}, \quad f_{n0} = f\sqrt{L\,|\bar{\beta}_2|}, \quad \text{and} \quad \delta_{n0} = \frac{\delta}{\alpha}, \qquad (1)$$

where D is the intra-cavity peak drive power, δ the frequency detuning, f is the filter bandwidth, L is the cavity length, α accounts for the cavity losses, γ is the nonlinear coefficient, and is $\overline{\beta_2}$ the average group-velocity dispersion (GDD divided by L). If chirped dissipative solitons are known to be stable in a particular cavity with specific values of normalized drive (D_{n0}), bandwidth (f_{n0}), and detuning (δ_{n0}) coefficients, stable chirped solitons (with peak power and duration scaled appropriately) can also be obtained for a different cavity as long as the values for the unitless coefficients do not change. While chirped pulses may be stable for many different values of these parameters, only one set is needed for design. The first relationship from Eq. (1) reveals that the required drive power has an inverse linear dependence on the total cavity nonlinearity (see Supplement 1, Section 12). The second relationship conveys that the filter bandwidth must scale inversely with the square root of the total GDD (see Supplement 1, Section 7). Note that the spectral bandwidth of the solution can be made arbitrarily broad with the appropriate choice filter. The third relationship suggests that the same solution can be recovered if the relative drive frequency scales linearly with the cavity loss. The use of the approximate mean-field model is validated by the confirmation of Eq. (1) qualitatively through full numerical simulations (see

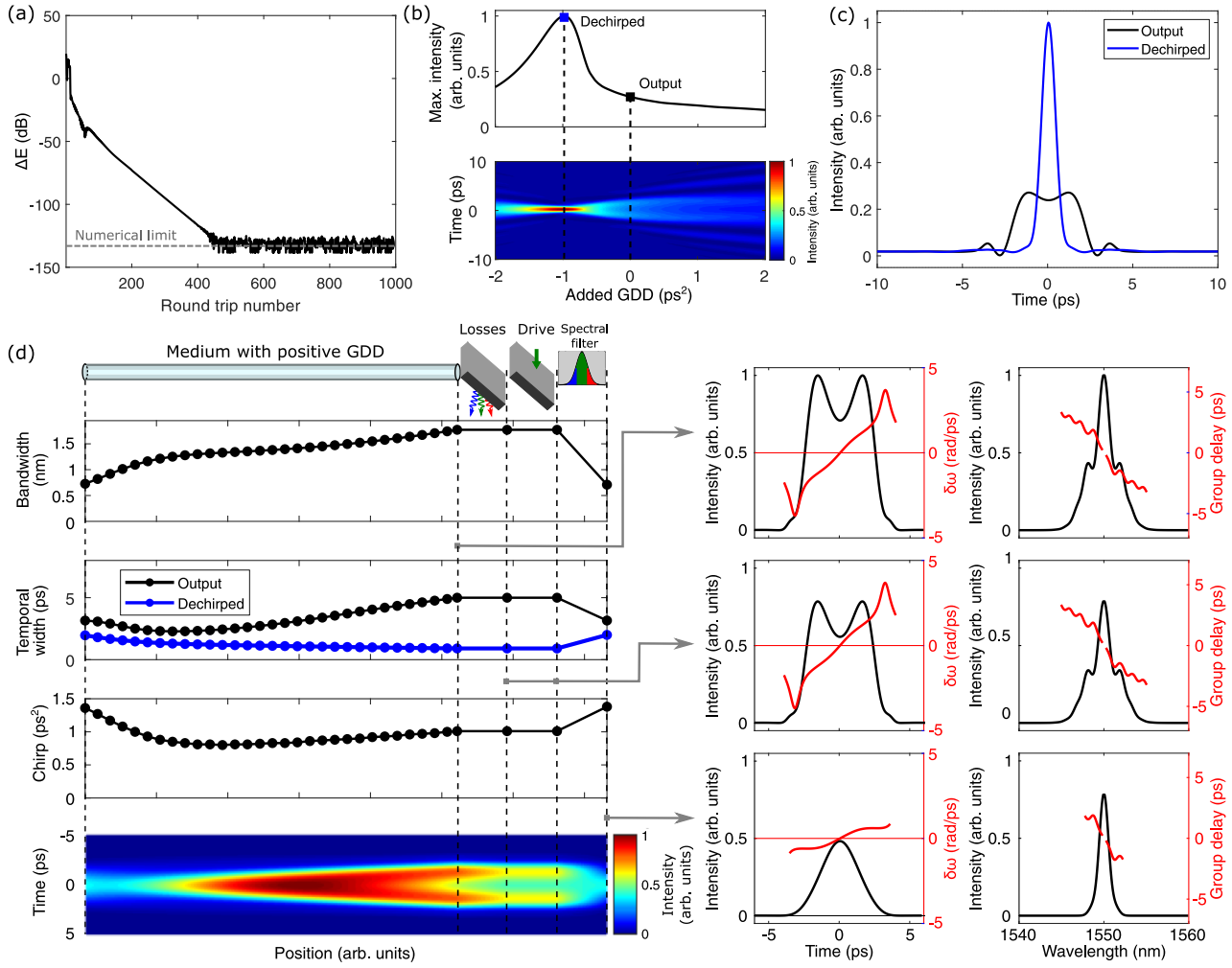

Fig. 2. Characteristics of chirped dissipative solitons in driven optical cavities. (a) Numerical convergence of the pulse energy difference between subsequent round trips, ΔE, to a stable numerically limited steady-state value. (b) Change in the pulse and peak intensity as a function of group-delay dispersion (GDD) applied after the cavity, indicating continuous compression with anomalous dispersion with a maximum at GDD $= -1$ ps^2. (c) Chirped cavity output (black) and dechirped (blue) pulses from (b). (d) Evolution of steady-state chirped dissipative soliton bandwidth [full width at half-maximum, (FWHM)], temporal width (FWHM), chirp (defined by the GDD required to maximize the pulse intensity, with the opposite sign), and pulse intensity in the cavity. The FWHM of the pulse after dechirping the pulse at each position of the cavity is plotted in blue. The associated pulse intensity, instantaneous frequency, power spectrum, and group delay from the indicated locations in the cavity are plotted on the right. The positive slope of the instantaneous frequency, $\delta\omega$, and the negative slope of the spectral group delay correspond to the soliton chirp.

Supplement 1, Sections 7 and 12). These simple relationships provide general design guidelines for obtaining chirped-pulse solitons in normal-dispersion driven cavities with a filter.

The chirped dissipative solitons observed numerically require drive powers that are challenging to obtain experimentally [Fig. 1(b)]. Numerically, while stable solutions can be obtained with low drive powers, they exist over a narrow range of parameters and may be challenging to observe in practice. In contrast, at higher drive powers, chirped pulses are stable over a large range of detuning values and may be more readily observed. This is the case, for example, in the all-normal dispersion cavity simulated in Fig. 1(b), with 10 W of intra-cavity drive power. However, since we are experimentally limited to 0.05 W of intra-cavity drive power by a 2 W average optical power amplifier, an advance is needed. Therefore, to experimentally observe chirped solitons, we design the cavity to have a reduced drive threshold power and achieve higher drive powers with a pulsed drive source. Driving passive cavities with pulses is a recently established technique for achieving higher peak drive powers [12,52,53]. For this technique, the continuous-wave drive is modulated into a nanosecond pulse with the repetition rate of the cavity, and then amplified. The peak drive power increases by an amount that corresponds to the duty cycle of the drive pulse train (drive pulse duration divided by the cavity round trip time). The drive pulse duration is fixed and, since the cavity round trip time increases linearly with the cavity length, the duty cycle decreases linearly, and, therefore, also the drive power increases linearly with cavity length (see Supplement 1, Section 13). In addition, Eq. (1) reveals that the required drive power threshold can be reduced linearly with an increase in the total cavity length. Considering both the reduced threshold power and the increased drive power, we find that stable chirped pulses should be observable for cavity lengths longer than 150 m, which corresponds to a threefold increase in drive power and a threefold decrease in drive power threshold [Fig. 1(c)]. However, an

increased cavity length would also increase the total dispersion, with a corresponding reduction in the bandwidth of the output pulse (see Supplement 1, Section 11). To avoid this loss of bandwidth, the length of the cavity is increased without changing the total dispersion with a dispersion-map consisting of two fibers with opposite signs of dispersion (dispersion management). A dispersion-managed approach allows for independent control of the drive power threshold in driven fiber resonators.

A suitable dispersion-managed fiber cavity is numerically modeled to confirm that chirped dissipative solitons are stable in an experimentally compatible system. To more accurately represent experimental parameters, the exact super-Gaussian profile of the bandpass spectral filter and the third-order dispersion of the fibers are incorporated in the model. Simulations are run for a 150 m cavity with the same total dispersion as in the all-normal dispersion cavity from Fig. 1(b). With only subtle differences from the all-normal dispersion system (see details in Supplement 1, Section 8), the drive power threshold scales as expected, and stable chirped dissipative solitons are observed with experimentally accessible peak drive powers of ∼3 W [Fig. 1(d)]. The numerical results validate the dispersion-managed cavity approach and motivate experimental investigation.

B. Experiment

Following the results of numerical simulations, a fiber resonator is designed to support chirped dissipative solitons [see Fig. 3(a) and Supplement 1, Sections 1 and 2]. The cavity consists of 150 m total

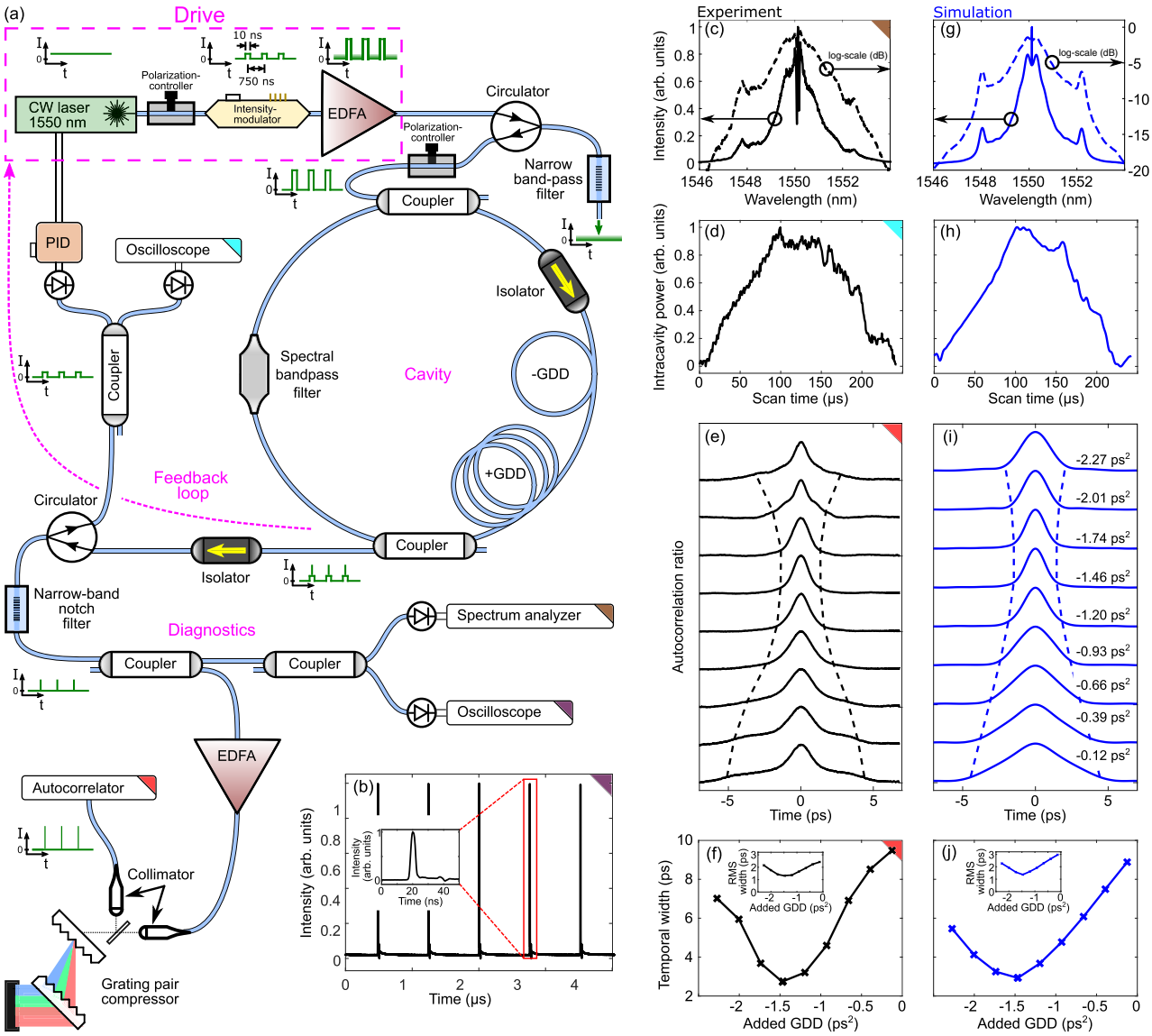

Fig. 3. Experimental schematic and observations of chirped dissipative solitons. (a) Experimental schematic depicting the modulated and amplified drive, the fiber cavity, the drive feedback loop, and diagnostics. The temporal waveform intensity is indicated throughout in green. Experimentally observed (b) pulse train, (c) spectrum, (d) cavity resonance with 0.9 W incident average power, and (e), (f) autocorrelation measurements. The resonance sweep is measured after a narrow bandpass filter, and the spectrum, pulse train, and autocorrelations are measured after a corresponding narrowband notch filter. Autocorrelations are measured after amplification as a function of the GDD from a grating pair compressor with the temporal pulse width ($1/e^2$ of the maximum width with the root mean square width inset) plotted in (f). A colored triangle in the upper right corner of the experimental data indicates the location and type of equipment used to obtain it with a matching triangle in the schematic. Comparable results from numerical simulations are plotted for the (g) spectrum, (h) resonance sweep, and (i), (j) autocorrelation measurements in blue.

length of single-mode fiber with large net-normal dispersion and a 4.25 nm fiber-format spectral filter. The drive is pulsed to enable access to high intra-cavity powers. The cavity resonance deviates significantly from a Lorentzian profile at incident average drive powers larger than 0.15 W, indicating the nonlinear nature of the resonance [Fig. 3(d)]. The equivalent numerical resonance agrees well with the experiment [Fig. 3(h)]. See Supplement 1, Sections 1, 2 and 14 for additional information.

Stable and reproducible chirped-pulse solutions are obtained with adjustment of the drive frequency, power, polarization, and pulse period as follows. With 0.9 W of average drive power incident on the cavity, the pump pulse period is matched to the 1.33 MHz repetition rate of the cavity, and the drive frequency (detuning) and polarization are swept through their range until broad-bandwidth, stable mode-locking is achieved. The polarization and detuning are varied in a process similar to that in fiber lasers mode-locked with nonlinear polarization evolution, in which three or four polarization wave plates are rotated through their range until stable mode-locking is achieved. The stable output optical spectrum features a unique profile characteristic of the simulated chirped pulses from region (ii) in Fig. 1(d) [Fig. 3(c)]. The spectra quantitatively agree with theory including small sidebands 2 nm shifted from the center wavelength and an rms bandwidth of 1.2 nm [Fig. 3(g)]. Small variations of these values can also be observed. The spectrum is measured after a fiber Bragg filter, resulting in the modulation in the center of the spectrum. The pulse train, observed with an oscilloscope, consists of pulses regularly spaced in time with the cavity round trip period and energy fluctuations of less than 0.7% [Fig. 3(b)]. To evaluate the output pulse chirp, the pulses are amplified and dechirped by a grating pair compressor and measured with a collinear intensity autocorrelator (see Supplement 1, Section 15). The autocorrelation width reduces to a minimum value before increasing again with further application of anomalous dispersion, which indicates positive chirp [Figs. 3(e) and 3(f)]. This change in duration on application of quadratic spectral phase also indicates a stable spectral phase, in contrast to noisy incoherent fields for which a autocorrelation measurement yields a coherence spike that does not respond to the application of a grating pair compressor (such as in Refs. [46,47]). The minimum duration (1.08 ps FWHM) corresponds to a GDD of 1.5 ps^2, which is 3 times the cavity GDD and indicates that the chirp is the result of nonlinear pulse formation. Comparable autocorrelations of numerically simulated chirped dissipative solitons agree well with the experimental observations [Figs. 3(i) and 3(j)].

3. DISCUSSION

The presented theoretical model does not account for the role of polarization dynamics in the cavity. Interactions between distinct polarizations can lead to modulation instability, which will affect the initiation of pulses in the cavity [54,55]. Polarization dynamics can also lead to intensity-dependent losses and are likely to influence pulse formation. Experiments suggest the relevance of polarization dynamics because pulse initiation and the character of the steady-state solutions are affected by the orientation of the polarization controllers. It will be valuable to account for the effects of polarization with a vectorized numerical model, which includes the orthogonal fiber polarization states as well as linear and nonlinear coupling [47,56]. Experimentally, additional stability and control of the solutions may be obtained by using a polarization controller in the single-mode fiber cavity or by replacing the single-mode cavity fiber with polarization-maintaining fiber.

Chirped dissipative solitons in normal dispersion resonators with a spectral filter are related to previously investigated nonlinear solutions in resonators without a filter as well (see Supplement 1, Section 16). At low powers in the fiber resonator and the LLE, dark pulses with a well-defined single trough are stable [33,35]. At higher drive powers and detuning values, the width and complexity of the dark pulse increases. Complex dark pulses with a long duration appear less like dark pulses and more like interlocking switching waves, which has been established as the theoretical basis for this class of solutions in the LLE [35]. At higher powers, dark pulses become unstable in the LLE and in simulations of the fiber cavity. However, when a weak spectral filter is added to the resonator (a 20 nm bandwidth for the 52.5 m cavity considered here), the long complex dark pulses (switching waves) begin to shift in parameter space and are stable at an order of magnitude higher powers. With a stronger 4 nm filter, the switching waves shift to even higher drive powers. With this strong filter, chirped pules begin to become stable along the same line in parameter space, but at drive powers that are as much as a hundred times higher than the powers needed for dark pulses in resonators without a filter. These bright pulses can no longer be interpreted as long-duration dark pulses because they have a well-defined pulse width, which is maintained regardless of the number of pulses observed. The bandwidth of the chirped pulse is broad compared to the other solutions, and the spectral phase has a clear quadradic component, which defines the chirp. However, while these solutions are distinguished from dark pulses, the interlocking switching-wave description may be relevant and merits further investigation. Interestingly, chirped-pulse solitons in mode-locked lasers can also be interpreted as the intersection of switching-wave solutions. The cubic-quintic Ginzburg–Landau equation that governs mode-locked lasers possesses chirped-pulse solutions that are well described analytically by the intersection of two propagating front solutions [57]. This common description may relate chirped dissipative solitons in passive resonators to chirped solitons in mode-locked lasers further, in addition to their comparable chirp, parameter requirements, and evolution. Further research into the formation and stability mechanisms of chirped dissipative solitons in passive cavities and their relationship to other normal dispersion solutions is needed.

In addition to strong spectral filtering, bright pulse solutions can also be enabled in the normal dispersion regime through interactions between different transverse mode families [39,41] as well as through higher-order dispersive and Raman interactions [58–61]. For example, in Ref. [58], bright pulse solutions are demonstrated through driving in the normal dispersion regime, with a strong contribution from higher-order dispersion. In this case, although the drive is in the normal dispersion regime, the pulse resides predominantly in the anomalous dispersion regime due to a spectral recoil induced by dispersive wave emission. In contrast, through strong spectral filtering, stable pulse formation is possible at very large net dispersion through the unique mechanisms described here. Spectral filtering enables highly chirped pulses for which nonlinear phase is directly compensated by normal dispersion. In addition, unlike bright pulses formed through alternate mechanisms, chirped pulses are stable despite large dissipation and can exhibit large intra-cavity dynamics.

Chirped dissipative solitons in normal dispersion resonators with a spectral filter have a higher drive threshold power than traditional solitons. In this work, chirped pulses were observed with 2 W

of average power (before the cavity), through the combination of a long fiber cavity and a pulsed drive. However, certain applications may require smaller average powers for pulse (comb) generation. The peak power of the drive is determined by the average power times the ratio of the drive pulse duration over the cavity round trip time. This peak power is currently limited by the duration of the drive pulse, which is limited by our pulse generator to >10 ns. This duration can be decreased to 100 ps with a suitable generator, which will decrease the average power threshold of the system by 2 orders of magnitude. In addition, the threshold power can be decreased further with narrower bandwidth spectral filters (see Supplement 1, Section 7). With both improvements, chirped dissipative solitons can be generated in fiber resonators with mW drive power.

Broad bandwidth is important for the frequency comb as well as for ultrashort pulse applications. The chirped pulses observed here have bandwidth corresponding to picosecond pulse durations. The soliton bandwidth can be increased by decreasing the total dispersion and by applying a correspondingly larger bandwidth spectral filter (see Supplement 1, Section 7). The scaling laws predict that the soliton bandwidth increases in proportion to the inverse of the square root of the cavity GDD if the spectral filter bandwidth is increased with the same proportion. In other words, 10 times broader soliton bandwidth should be possible with a cavity GDD that is 100 times smaller and a spectral filter with 10 times broader bandwidth than the present configuration.

For a given bandwidth, the energy of the pulse determines important parameters for applications, including the pulse peak power, the frequency comb power-per-comb line, and the conversion efficiency. Since chirped solitons in mode-locked lasers have higher energies than solitons in anomalous dispersion laser cavities, it will be important to determine if a similar benefit can be achieved for passive cavities. In passive cavities, the pulse energy is challenging to measure accurately because it is difficult to accurately determine the total number of pulses and residual continuous-wave background complicates the interpretation of average power measurements. These challenges can potentially be addressed through seeding the cavity with an external source and with background management techniques; this is the subject of ongoing research. In addition, numerical simulations can provide important information about the pulse energy, including the potential enhancements compared to traditional solitons and opportunities for further increases (see Supplement 1, Section 17). For example, the energy of the simulated chirped solitons corresponding to experimental observations is 25 pJ. In a controlled numerical comparison between traditional solitons in anomalous dispersion cavities and chirped solitons in normal dispersion cavities, we find that chirped pulses can have at least seven times more energy (see Supplement 1, Section 17, Fig. S16). By driving normal dispersion resonators with higher powers, the energy of stable chirped dissipative solitons can be increased by at least 2 times more. Alternatively, optimizing for peak power instead of energy, we find that chirped dissipative solitons can support at least an order of magnitude higher peak powers than traditional solitons given an equivalent magnitude of GDD. The simulated results are encouraging, highlight the promise of chirped dissipative solitons for applications, and motivate further research.

In passive resonators, the resonance frequencies are sensitive to environmental perturbations including vibrations and temperature. Moreover, the drive laser frequency must be locked with respect to these resonances. Therefore, the stability of frequency comb generation is proportional to the strength of environmental perturbations and the quality of the frequency locking mechanism. The resonator investigated in this study features minimal temperature and vibration control, a limited laser frequency tuning range, a free-running drive repetition rate, and a single-stage side-lock proportional–integral–derivative (PID) controller feedback loop. Stable frequency comb generation in this nonideal configuration lasts for several minutes. However, with several improvements, including temperature and vibration control, an additional feedback loop to control for large frequency changes by thermally tuning the laser, locking the drive repetition rate to the cavity, and peak-locking techniques, stable frequency combs should be generated over significantly longer periods, with minimal variation.

Stretched-pulse mode-locking has been recently demonstrated in a fiber Kerr resonator [62] after the results from the present manuscript were posted as a preprint [63]. The stretched-pulse and chirped-pulse regimes of operation are each characterized by clear qualitative features in the system itself as well as in the pulsed solutions, are readily distinguished, and possess unique practical benefits. The stretched-pulse regime requires two sections of fiber with near equal dispersion but with opposite signs and a total dispersion that is slightly anomalous, in contrast to the large normal dispersion and lack of need for anomalous dispersion for the chirped pulses. Chirped-pulse temporal and spectral profiles are critically dependent on the application of a spectral filter, and without the presence of a spectral filter, no chirped pulses are stable at all (Supplement 1, Section 7). In contrast to chirped pulses, stretched pulses are uniquely defined by their Gaussian spectral and temporal profiles. Stretched pulses stretch and compress twice, the chirp is both positive and negative, and the pulse is transform-limited twice in the cavity whereas chirped pulses only increase in duration once, have only high and positive chirp, and are never transform-limited in the cavity. Stretched-pulse solitons balance nonlinear phase with the net effective anomalous dispersive phase in the cavity whereas chirped pulses balance both amplitude and phase modulations with the pulse chirp enabling the dispersion to have both amplitude and phase contributions in the time domain and the nonlinearity to have both amplitude and phase contributions in the spectral domain. The filter plays a critical role in completing this amplitude and phase balance for the chirped pulse (see Supplement 1, Section 9 for complete details). Regarding benefits for applications, stretched pulses enable ultrashort pulsed performance because the total dispersion is near zero and chirped pulses can tolerate more than an order of magnitude higher pulse energies, as detailed in Supplement 1, Section 17.

Chirped dissipative solitons represent a new class of stable nonlinear waveforms in driven resonators that enable opportunities for nonlinear pattern formation and enhanced performance regimes for frequency comb and ultrashort pulse generation and associated applications. The present study focuses specifically on fiber resonators, but the results are general and can be applied to any passive resonator platform using the scaling laws given by Eq. (1). Chirped dissipative solitons enable enhanced performance for microcomb devices and enable femtosecond pulse generation in fiber at wavelengths not accessible by traditional mode-locked lasers. For bulk enhancement cavities, chirped dissipative solitons can enhance the performance of high harmonic generation and pulse compression at higher energy levels. Finally, stable dissipative

soliton formation in the presence of large dissipation motivates investigations of qualitative new phenomena including dissipative soliton resonances and intra-cavity soliton explosions in simple passive resonators.

Funding. National Institute of Biomedical Imaging and Bioengineering (R01EB028933).

Disclosures. The authors declare no conflicts of interest.

Data Availability. Data underlying the results presented in this paper are not publicly available at this time but may be obtained from the authors upon reasonable request.

Supplemental document. See Supplement 1 for supporting content.

REFERENCES

1. N. Akhmediev and A. Ankiewicz, *Dissipative Solitons: From Optics to Biology and Medicine* (Springer Berlin Heidelberg, 2008).
2. H. G. Purwins, H. U. Bodeker, and S. Amiranashvili, "Dissipative solitons," Adv. Phys. **59**, 485–701 (2010).
3. P. Del'Haye, T. Herr, E. Gavartin, M. L. Gorodetsky, R. Holzwarth, and T. J. Kippenberg, "Octave spanning tunable frequency comb from a microresonator," Phys. Rev. Lett. **107**, 063901 (2011).
4. Y. K. Chembo and N. Yu, "On the generation of octave-spanning optical frequency combs using monolithic whispering-gallery-mode microresonators," Opt. Lett. **35**, 2696–2698 (2010).
5. Y. Okawachi, K. Saha, J. S. Levy, Y. H. Wen, M. Lipson, and A. L. Gaeta, "Octave-spanning frequency comb generation in a silicon nitride chip," Opt. Lett. **36**, 3398–3400 (2011).
6. T. J. Kippenberg, A. L. Gaeta, M. Lipson, and M. L. Gorodetsky, "Dissipative Kerr solitons in optical microresonators," Science **361**, eaan8083 (2018).
7. A. L. Gaeta, M. Lipson, and T. J. Kippenberg, "Photonic-chip-based frequency combs," Nat. Photonics **13**, 158–169 (2019).
8. M. Nakazawa, K. Suzuki, and H. Haus, "Modulational instability oscillation in nonlinear dispersive ring cavity," Phys. Rev. A **38**, 5193–5196 (1988).
9. M. Haelterman, S. Trillo, and S. Wabnitz, "Additive-modulation-instability ring laser in the normal dispersion regime of a fiber," Opt. Lett. **17**, 745–747 (1992).
10. M. Haelterman, S. Trillo, and S. Wabnitz, "Dissipative modulation instability in a nonlinear dispersive ring cavity," Opt. Commun. **91**, 401–407 (1992).
11. J. K. Jang, M. Erkintalo, S. G. Murdoch, and S. Coen, "Ultraweak long-range interactions of solitons observed over astronomical distances," Nat. Photonics **7**, 657–663 (2013).
12. M. Anderson, F. Leo, S. Coen, M. Erkintalo, and S. G. Murdoch, "Observations of spatiotemporal instabilities of temporal cavity solitons," Optica **3**, 1071–1074 (2016).
13. J. K. Jang, M. Erkintalo, S. Coen, and S. G. Murdoch, "Temporal tweezing of light through the trapping and manipulation of temporal cavity solitons," Nat. Commun. **6**, 7370 (2015).
14. F. Leo, S. Coen, P. Kockaert, S. P. Gorza, P. Emplit, and M. Haelterman, "Temporal cavity solitons in one-dimensional Kerr media as bits in an all-optical buffer," Nat. Photonics **4**, 471–476 (2010).
15. J. K. Jang, M. Erkintalo, J. Schroder, B. J. Eggleton, S. G. Murdoch, and S. Coen, "All-optical buffer based on temporal cavity solitons operating at 10 Gb/s," Opt. Lett. **41**, 4526–4529 (2016).
16. M. Haelterman, S. Trillo, and S. Wabnitz, "Hopf sideband bifurcation and chaos in fiber lasers with injected signal," Phys. Rev. A **47**, 2344–2353 (1993).
17. J. S. Levy, A. Gondarenko, M. Foster, A. C. Turner-Foster, A. L. Gaeta, and M. Lipson, "CMOS-compatible multiple-wavelength oscillator for on-chip optical interconnects," Nat. Photonics **4**, 37–40 (2009).
18. L. Razzari, D. Duchesne, M. Ferrera, R. Morandotti, S. Chu, B. E. Little, and D. J. Moss, "CMOS-compatible integrated optical hyper-parametric oscillator," Nat. Photonics **4**, 41–45 (2010).
19. P. Del'Haye, A. Schliesser, O. Arcizet, T. Wilken, R. Holzwarth, and T. J. Kippenberg, "Optical frequency comb generation from a monolithic microresonator," Nature **450**, 1214–1217 (2007).
20. A. Savchenkov, A. Matsko, V. Ilchenko, I. Solomatine, D. Seidel, and L. Maleki, "Tunable optical frequency comb with a crystalline whispering gallery mode resonator," Phys. Rev. Lett. **101**, 093902 (2008).
21. T. Herr, V. Brasch, J. D. Jost, C. Y. Wang, N. M. Kondratiev, M. L. Gorodetsky, and T. J. Kippenberg, "Temporal solitons in optical microresonators," Nat. Photonics **8**, 145–152 (2014).
22. N. Lilienfein, C. Hofer, M. Högner, T. Saule, M. Trubetskov, V. Pervak, E. Fill, C. Riek, A. Leitenstorfer, J. Limpert, F. Krausz, and I. Pupeza, "Temporal solitons in free-space femtosecond enhancement cavities," Nat. Photonics **13**, 214–218 (2019).
23. V. L. Kalashnikov, "Femtosecond pulse enhancement in an external resonator: impact of dispersive and nonlinear effects," Appl. Phys. B **92**, 19–23 (2008).
24. L. F. Mollenauer and R. H. Stolen, "The soliton laser," Opt. Lett. **9**, 13–15 (1984).
25. S. Coen and M. Erkintalo, "Universal scaling laws of Kerr frequency combs," Opt. Lett. **38**, 1790–1792 (2013).
26. W. H. Renninger and P. T. Rakich, "Closed-form solutions and scaling laws for Kerr frequency combs," Sci. Rep. **6**, 24742 (2016).
27. A. Chong, J. Buckley, W. Renninger, and F. Wise, "All-normal-dispersion femtosecond fiber laser," Opt. Express **14**, 10095–10100 (2006).
28. W. Renninger, A. Chong, and F. Wise, "Dissipative solitons in normal-dispersion fiber lasers," Phys. Rev. A **77**, 023814 (2008).
29. A. Chong, W. H. Renninger, and F. W. Wise, "Properties of normal-dispersion femtosecond fiber lasers," J. Opt. Soc. Am. B **25**, 140–148 (2008).
30. W. H. Renninger, A. Chong, and F. W. Wise, "Pulse shaping and evolution in normal-dispersion mode-locked fiber lasers," IEEE J. Sel. Top. Quantum Electron. **18**, 389–398 (2012).
31. A. Chong, W. H. Renninger, and F. W. Wise, "All-normal-dispersion femtosecond fiber laser with pulse energy above 20 nJ," Opt. Lett. **32**, 2408–2410 (2007).
32. W. H. Renninger, A. Chong, and F. W. Wise, "Giant-chirp oscillators for short-pulse fiber amplifiers," Opt. Lett. **33**, 3025–3027 (2008).
33. C. Godey, I. V. Balakireva, A. Coillet, and Y. K. Chembo, "Stability analysis of the spatiotemporal Lugiato-Lefever model for Kerr optical frequency combs in the anomalous and normal dispersion regimes," Phys. Rev. A **89**, 063814 (2014).
34. D. C. Cole, E. S. Lamb, P. Del'Haye, S. A. Diddams, and S. B. Papp, "Soliton crystals in Kerr resonators," Nat. Photonics **11**, 671–676 (2017).
35. P. Parra-Rivas, D. Gomila, E. Knobloch, S. Coen, and L. Gelens, "Origin and stability of dark pulse Kerr combs in normal dispersion resonators," Opt. Lett. **41**, 2402–2405 (2016).
36. W. Liang, A. A. Savchenkov, V. S. Ilchenko, D. Eliyahu, D. Seidel, A. B. Matsko, and L. Maleki, "Generation of a coherent near-infrared Kerr frequency comb in a monolithic microresonator with normal GVD," Opt. Lett. **39**, 2920–2923 (2014).
37. B. Y. Kim, Y. Okawachi, J. K. Jang, M. Yu, X. Ji, Y. Zhao, C. Joshi, M. Lipson, and A. L. Gaeta, "Turn-key, high-efficiency Kerr comb source," Opt. Lett. **44**, 4475–4478 (2019).
38. X. Xue, Y. Xuan, Y. Liu, P. H. Wang, S. Chen, J. Wang, D. E. Leaird, M. Qi, and A. M. Weiner, "Mode-locked dark pulse Kerr combs in normal-dispersion microresonators," Nat. Photonics **9**, 594–600 (2015).
39. J. K. Jang, Y. Okawachi, M. Yu, K. Luke, X. Ji, M. Lipson, and A. L. Gaeta, "Dynamics of mode-coupling-induced microresonator frequency combs in normal dispersion," Opt. Express **24**, 28794–28803 (2016).
40. X. Xue, Y. Xuan, P. H. Wang, Y. Liu, D. E. Leaird, M. Qi, and A. M. Weiner, "Normal-dispersion microcombs enabled by controllable mode interactions," Laser Photon. Rev. **9**, L23–28 (2015).
41. V. E. Lobanov, G. Lihachev, T. J. Kippenberg, and M. L. Gorodetsky, "Frequency combs and platicons in optical microresonators with normal GVD," Opt. Express **23**, 7713–7721 (2015).
42. A. Fülöp, M. Mazur, A. Lorences-Riesgo, T. A. Eriksson, P.-H. Wang, Y. Xuan, D. E. Leaird, M. Qi, P. A. Andrekson, A. M. Weiner, and V. Torres-Company, "Long-haul coherent communications using microresonator-based frequency combs," Opt. Express **25**, 26678–26688 (2017).
43. B. Garbin, Y. Wang, S. G. Murdoch, G.-L. Oppo, S. Coen, and M. Erkintalo, "Experimental and numerical investigations of switching wave dynamics in a normally dispersive fiber ring resonator," Eur. Phys. J. D **71**, 240 (2017).
44. X. Xue, M. Qi, and A. M. Weiner, "Normal-dispersion microresonator Kerr frequency combs," Nanophotonics **5**, 244–262 (2016).

45. S. W. Huang, H. Zhou, J. Yang, J. F. McMillan, A. Matsko, M. Yu, D. L. Kwong, L. Maleki, and C. W. Wong, "Mode-locked ultrashort pulse generation from on-chip normal dispersion microresonators," Phys. Rev. Lett. **114**, 053901 (2015).
46. M. Erkintalo and S. Coen, "Coherence properties of Kerr frequency combs," Opt. Lett. **39**, 283–286 (2014).
47. S. Coulibaly, M. Taki, A. Bendahmane, G. Millot, B. Kibler, and M. G. Clerc, "Turbulence-induced rogue waves in Kerr resonators," Phys. Rev. X **9**, 011054 (2019).
48. W. Chang, A. Ankiewicz, J. M. Soto-Crespo, and N. Akhmediev, "Dissipative soliton resonances," Phys. Rev. A **78**, 23830 (2008).
49. J. M. Soto-Crespo, N. Akhmediev, and A. Ankiewicz, "Pulsating, creeping, and erupting solitons in dissipative systems," Phys. Rev. Lett. **85**, 2937–2940 (2000).
50. S. T. Cundiff, J. M. Soto-Crespo, and N. Akhmediev, "Experimental evidence for soliton explosions," Phys. Rev. Lett. **88**, 739031 (2002).
51. W. H. Renninger and F. W. Wise, "Fiber lasers," in *Dissipative Soliton Fiber Lasers* (Wiley-VCH Verlag GmbH & Co. KGaA, 2012), pp. 97–133.
52. E. Obrzud, S. Lecomte, and T. Herr, "Temporal solitons in microresonators driven by optical pulses," Nat. Photonics **11**, 600–607 (2017).
53. M. Malinowski, A. Rao, P. Delfyett, and S. Fathpour, "Optical frequency comb generation by pulsed pumping," APL Photon. **2**, 066101 (2017).
54. M. Haelterman, S. Trillo, and S. Wabnitz, "Polarization multistability and instability in a nonlinear dispersive ring cavity," J. Opt. Soc. Am. B **11**, 446–456 (1994).
55. J. Fatome, B. Kibler, F. Leo, A. Bendahmane, G.-L. Oppo, B. Garbin, S. G. Murdoch, M. Erkintalo, and S. Coen, "Polarization modulation instability in a nonlinear fiber Kerr resonator," Opt. Lett. **45**, 5069–5072 (2020).
56. G. P. Agrawal, *Nonlinear Fiber Optics* (Academic, 2007).
57. J. M. Soto-Crespo, N. N. Akhmediev, V. V. Afanasjev, and S. Wabnitz, "Pulse solutions of the cubic-quintic complex Ginzburg-Landau equation in the case of normal dispersion," Phys. Rev. E **55**, 4783–4796 (1997).
58. Z. Li, Y. Xu, S. Coen, S. Murdoch, and M. Erkintalo, "Experimental observations of bright dissipative Kerr cavity solitons and their collapsed snaking in a driven resonator with normal dispersion," Optica **7**, 1195–1203 (2020).
59. Y. Xu, A. Sharples, J. Fatome, S. Coen, M. Erkintalo, and S. G. Murdoch, "Frequency comb generation in a pulse-pumped normal dispersion Kerr mini-resonator," Opt. Lett. **46**, 512–515 (2021).
60. P. Parra-Rivas, S. Coulibaly, M. G. Clerc, and M. Tlidi, "Influence of stimulated Raman scattering on Kerr domain walls and localized structures," Phys. Rev. A **103**, 013507 (2020).
61. P. Parra-Rivas, D. Gomila, and L. Gelens, "Coexistence of stable dark- and bright-soliton Kerr combs in normal-dispersion resonators," Phys. Rev. A **95**, 053863 (2017).
62. X. Dong, Q. Yang, C. Spiess, V. G. Bucklew, and W. H. Renninger, "Stretched-pulse soliton Kerr resonators," Phys. Rev. Lett. **125**, 033902 (2020).
63. C. Spiess, Q. Yang, X. Dong, V. G. Bucklew, and W. H. Renninger, "Chirped temporal solitons in driven optical resonators," arXiv:1906.12127 (2019).